ADVANCED FUNCTIONAL MATERIALS
www.afm-journal.de

Electrically Driven Random Laser Memory

*Cih-Su Wang, Chuan-Hsien Nieh, Tai-Yuan Lin, and Yang-Fang Chen**

The first electrically driven random laser diode with nonvolatile resistive random access memory functionality is designed and demonstrated. To illustrate the working principle, a metal–insulator–semiconductor structure based on Pt/MgO/ZnO thin-film layers is fabricated on indium tin oxide glass. The current–voltage curve of the dual-function random laser memory (RLM) device exhibits an excellent electrical bistability with a high ON/OFF current ratio (≈10^7). The random lasing behavior is simultaneously demonstrated by using electrical pumping with the appearance of sharp-peak emissions and a drastic enhancement of peak intensity. A wide angle-dependent electroluminescence not only reveals its emitting advantage but also further supports the origin of random lasers. The first proof-of-concept presentation of RLM possesses several advantages of dual memory and lasing functions, which enables to open up new avenues to practical applications, such as light emitting memories for electrical and optical communication. This new horizon for the realization of all optical memories should therefore be able to attract academic as well as industrial interests. It is stressed here that the electrical reading of conventional memory array is usually in serial sequence, which limits the maximum data throughput. This hurdle can be overcome by optically readable memory devices.

1. Introduction

In the modern digital age, information communication and storage are now omnipresent and paramount for the functional enhancement. For conventional memory arrays, they are usually read by electrical signal under an applied external bias in series sequence, which greatly limits the data throughput. This difficulty can be circumvented by optically readable memory devices. In addition, for the realization of all-optical memory, an electrically operated memory element with optical output would open a true application horizon. In this paper, via the integration of resistance random access memory (RRAM) and random laser (RL), for the first time, we demonstrate an optically and electrically readable random laser memory (RLM). Among several types of memory devices, recent progress of RRAM has attracted great attention due to its potential for the replacement of Flash memory.[1–3] As next-generation nonvolatile memory applications, the metal–insulator–metal (MIM) module has been considered as promising storage element due to its merits of facile fabrication, low cost and 3D-stacked capability.[4] So far, various materials, such as metal oxides, and organic materials, have already been demonstrated to exhibit the properties of switchable resistance.[5–7] Although the underlying mechanism of RS behavior is not yet clearly understood, however, various models have been proposed, such as conducting filaments composed of metallic atoms, or oxygen vacancies, hopping conduction, and trap-controlled space-charge-limited current.[8–10] Among the binary metal oxides, zinc oxide (ZnO) and magnesium oxide (MgO) have been respectively investigated to show excellent memory properties via using thin film, nanorod, and nano-island structures.[8–13] ZnO is a promising functional material with a wide direct bandgap (3.37 eV) and large exciton binding energy (60 meV); it is biocompatible, highly chemical stable, and has excellent UV emission properties,[14] while MgO is a chemically inert material, which has a large bandgap (7.9 eV), high thermal conductivity, and high break-down field (≈12 MV cm^{-1}).[9] The accumulated advantages described above thus provide an ideal motivation for the exploration of resistance switching (RS) memory device based on ZnO/MgO composite.

Random lasing is a phenomenon that has been discovered based on a highly disordered gain medium that enables to amplify light when pumped externally, and the scattering strength is nearly constant within the gain spectrum of the active medium.[15,16] During the multiple and recurrent scattering process, which provide coherent feedback, laser action with wide angle distribution starts to emerge when the amplification exceeds the loss in an active random medium system.[17] In recent years, much more attention has been paid to this field due to its various applications such as remote heat sensing, document encoding, and even medical diagnostics.[18–21] However, most random lasers are induced by optical pumping.[17,22,23] For practical applications, electrical pumping RL is now needed and starts to be realized in few types of ZnO-based heterojunctions.[18,24–26] Here, via using platinum (Pt), and indium tin oxide (ITO) as top and bottom electrodes, a random laser diode in the form of Pt/MgO/ZnO/ITO can be achieved. In this metal–insulator–semiconductor (MIS) laser diode, ZnO nanocrystallite film not only plays the role of optical gain medium, but also serves as the active scattering feedback centers to

Dr. C.-S. Wang, C.-H. Nieh, Prof. Y.-F. Chen
Department of Physics
National Taiwan University
Taipei 106, Taiwan
E-mail: yfchen@phys.ntu.edu.tw
Prof. T.-Y. Lin
Institute of Optoelectronic Sciences
National Taiwan Ocean University
Keelung 202, Taiwan

DOI: 10.1002/adfm.201500734

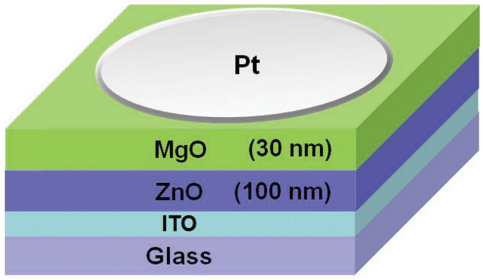

Figure 1. Schematic illustration of RLM in the structure of Pt/MgO/ZnO/ITO.

generate the lasing action. Therefore, the newly designed Pt/MgO/ZnO/ITO device possesses two functionalities, including laser action and data storage. To the best of our knowledge, there is no early report has ever discussed the potential and possibility of generating memory function from the electrically driven random laser diode. The discovery of RLM shown here can open up a new avenue toward electrical and optical communication, which should further generate both academic study and practical applications.

2. Results and Discussion

The schematic illustration of the designed RLM (Pt/MgO/ZnO/ITO) structure is shown in **Figure 1**. A typical scanning electron microscope (SEM) topography of ZnO films, which is used as random laser media here, is shown in **Figure 2**a. It can be clearly seen that the films consist of nano-crystallites with the grain size ranging from 30 to 60 nm. As reported previously, the optical gain of nano-crystalline ZnO is an order of magnitude larger than that of the bulk ZnO, thus favors the realization of lasers.[25] To confirm the existence of ZnO material, an X-ray diffraction (XRD) is performed in Figure 2b, in which the peak centered at 34.48° can be well indexed to the diffraction from (0002) facet of wurtzite ZnO.[25] The XRD information indicates that the obtained ZnO layer is hexagonal-wurtzite structured with a *c*-axis preferred orientation.[27] For the optical characterization, the PL spectra of the ZnO films with and without annealing are shown in Figure 2c. The UV peak located at the position of 380 nm corresponds to the near-band-edge emission (NBE), while the visible spectrum centered at around 500 nm is attributed to the deep-level emission (DLE) due to the high density of inherent oxygen defects.[10] The PL spectra thus serve as additional evidence to support the existence of ZnO films. Furthermore, via effective annealing at 300 °C for 1 h, the NBE derived from ZnO layer can be sufficiently enhanced, while the DLE is efficiently suppressed, thus favors the realization of UV lasing behavior.

Figure 3a shows the typical *I*–*V* characteristics of the RLM device. The arrows in the figure indicate the sweeping direction of applying voltage. Once the applied voltage exceeded a turn-on voltage of +9.8 V, a rapid increase in the current was observed. The threshold voltage triggers the RLM cell from high resistance state (HRS) to low resistance state (LRS), which is defined as the "SET" process. The switch from low- (OFF) to high-conductivity (ON) state is equivalent to the "writing"

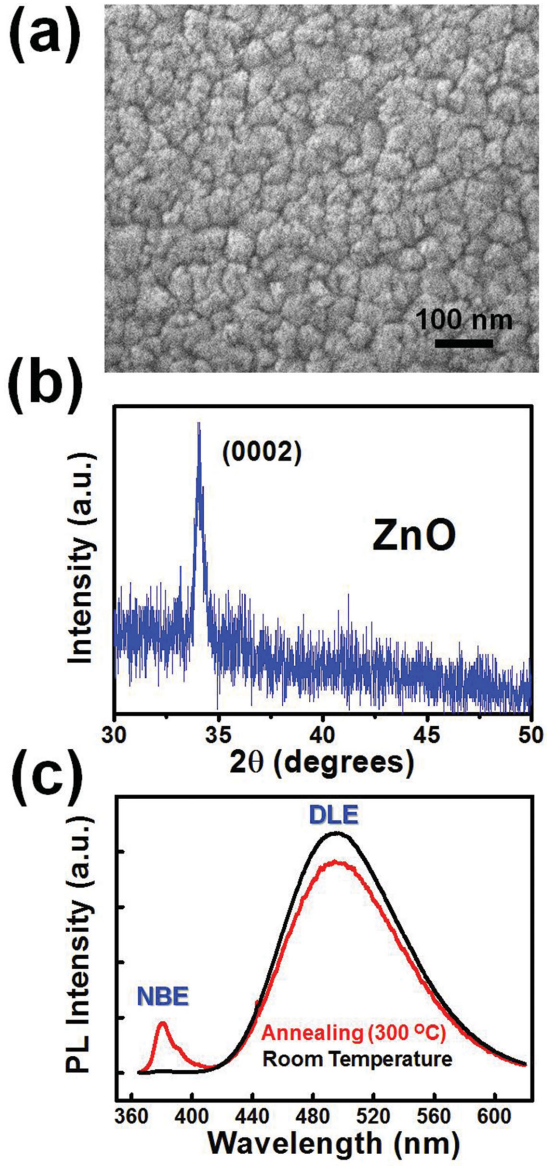

Figure 2. a) Scanning electron microscope (SEM) image, b) X-ray diffraction (XRD), and c) photoluminescence (PL) spectra of ZnO nanocrystallite films grown on ITO glass.

command to a digital storage device.[4] Meanwhile, a high ON/OFF current ratio of ≈10^7 (read at +1 V), which promises a low misreading probability in data access, is shown in Figure 3b as well. Furthermore, the ON state can be well remained even when the power was off, indicating a nonvolatile memory feature of the RLM. The LRS (ON) was not retrievable by applying a reverse bias. In Figure 3c, the high conductivity remained as the voltage sweeping from 0 to −10 V and −10 to 0 V. These features thus indicate the designed RLM is a write-once-read-many (WORM)-type memory device.[4] In addition to the low misreading probability, the device stability is also important. To test the data retention ability, the LRS/HRS was probed at regular time interval under a reading voltage of +1 V. Observed from **Figure 4**, both the LRS and HRS remained in the same order of magnitude with a considerable duration of more than

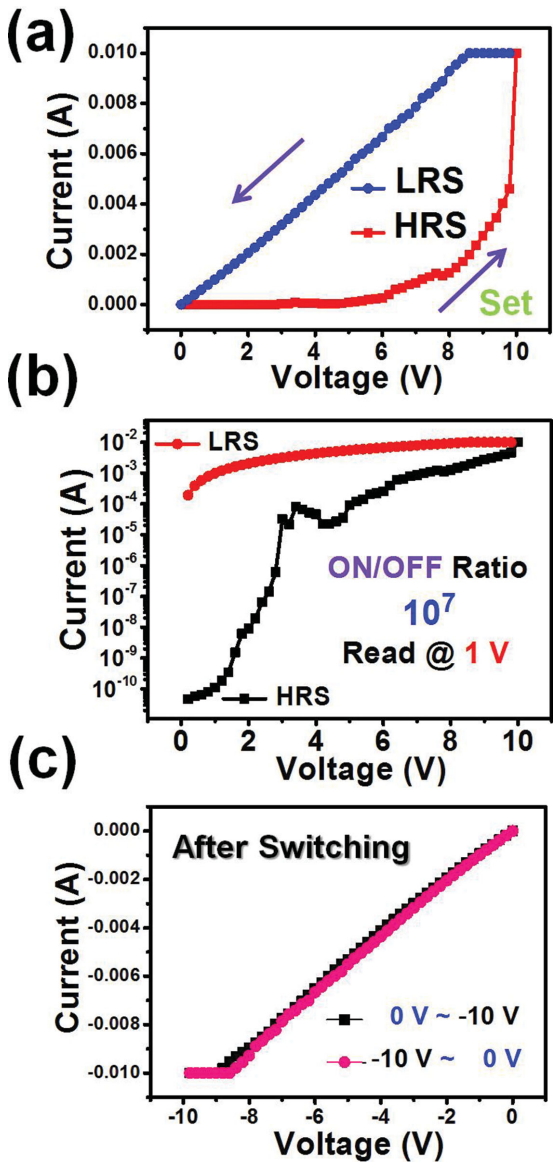

Figure 3. *I–V* characteristics a) without and b) with log function of current (*I*) axis. c) *I–V* characteristics of RLM after switching from high resistance state (HRS) to low resistance state (LRS).

10^3 s. Therefore, an excellent stability of the RLM device is further confirmed for practical applications.

The underlying origin of the RS in RLM device is intriguing but still controversial. Nevertheless, the measured *I–V* characteristic reveals a possible underlying mechanism. According to the previous reports,[3,4,5,10] the two main mechanisms responsible for the transport behaviors in RRAM devices are the formation of conducting filaments and charge trapping effects. For the mechanism of conducting filaments, as the applied bias is increased, the induced electric field will lure the metal particles into the dielectric layer from electrodes. Under an intense electric field, conducting bridges can be grown in the dielectric layer. Consequently, the memory switches from a low-conductivity state to a high-conductivity state. When a negative bias is applied across the device, the joule heating can fracture the

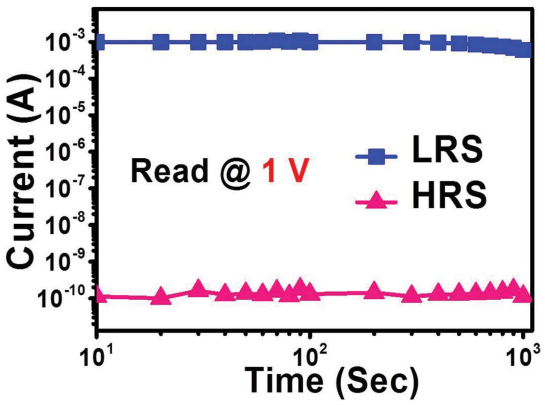

Figure 4. Programmed data retention ability at a reading voltage of +1 V before and after switching, respectively.

conducting bridges and recover the memory to the low-conductivity state. Therefore, if the working principle of the memory follows the conducting filament mechanism, the switching behavior is rewritable.[3] On the other hand, if the underlying mechanism responsible for the memory is due to charge trapping effects, the switching behavior is not retrievable as shown in previous studies.[4] It is because the trapping barrier is usually very large (≥0.5 eV), and the applied negative bias is not able to sweep trapped charges out of the dielectric layer. Obviously, in our case, since the ON state is not retrievable, this behavior may thus reflect the possibility that the mechanism responsible for the RS effect arises from charge trapping as shown in our previous publications.[3,4]

The advantage of the newly designed RLM device is based on its dual functional abilities. In addition to the RS effect, an electrically driven RL action can also be well observed. **Figure 5** shows the evolution of electroluminescence (EL) spectra with an increase of positive driving current. At a low injection current such as 10 mA, the EL spectrum, which can be attributed to the spontaneous emission is broad, relatively weak and partially spoiled by background noise. However, when the driving current exceeds a specific threshold above 30 mA, such as 47 mA, sharp peaks with FWHM less than 0.8 nm start to emerge and superpose on the broad spontaneous emission. By further increasing the injection current to 62 and 77 mA, more sharp peaks appear. The appearance of randomly distributed

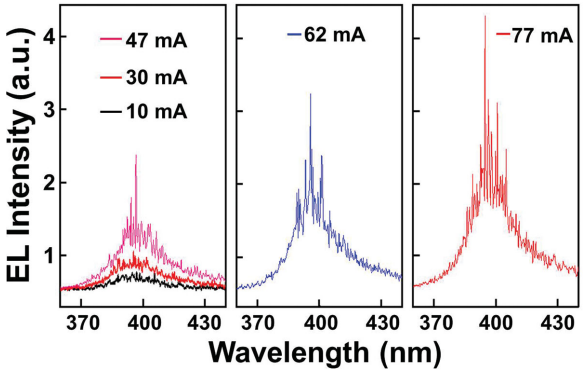

Figure 5. Lasing characterization of RLM by electrical pumping under different positive injection current.

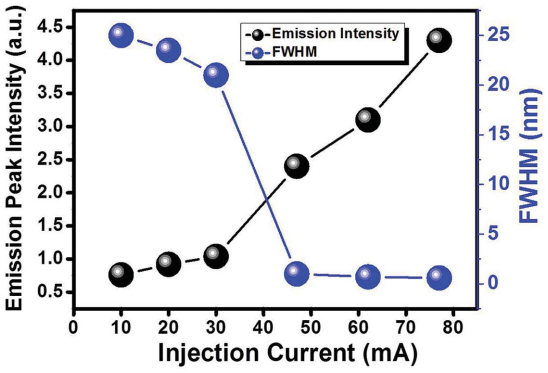

Figure 6. EL intensity and full width at half maximum (FWHM) as functions of injection current.

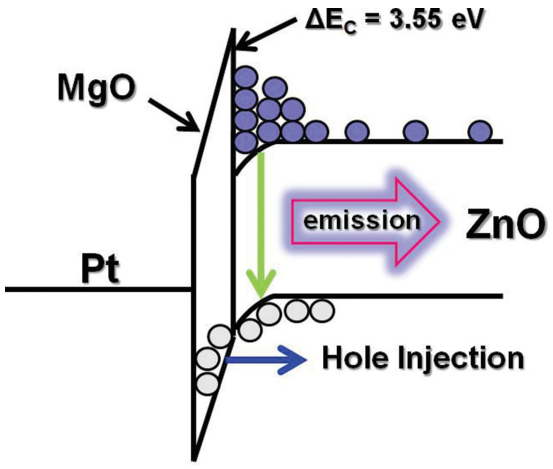

Figure 7. The RLM diode (Pt/MgO/ZnO) is operated under forward bias.

sharp peaks with very narrow line width upon increasing current suggests that the typical random lasing behavior has been derived.[17] It is noted that the EL spectra is collected from the direction normal to the sample surface. The dependences of emission intensity and full width at half maximum (FWHM) versus injection current are shown in **Figure 6**, in which the threshold current is about 30 mA and the line width shows a significant reduction as the laser action starts to emerge. Since the thickness of the ZnO nano-crystallite film is about 100 nm, which is less than the half wavelength of the emitted UV light, the possibility of the Fabry–Perot type laser can be excluded. Random lasing is defined to be achieved when the excited light is multiply scattered in a closed-loop path till its amplification exceeds loss.[17] Hence, the ZnO nano-crystallite film, which has a high refractive index ($n \approx 2.45$) and multiple grains and voids are well feasible to form the random cavity, supporting the occurrence of RL. By using the information of the wavelength difference ($\Delta\lambda$) derived from the two nearest lasing peaks, the transport mean free path (L) of a light in the composite system can be further calculated by $L = \lambda^2/2n\Delta\lambda$,[28] where λ is the resonant wavelength (≈396 nm), n is the refractive index (≈2.45). The resultant approximate value is about 53.3 μm. Different output lasing modes and intensities can be instantly generated by the every moment changed closed-loop path. In our case, since the observed sharp emission peaks change randomly under each detection, these unique features therefore provide a firm evidence to support that our findings belong to the random laser behavior.

To better explore the EL origin, a band diagram of the Pt/MgO/ZnO laser diode is illustrated in **Figure 7**. The conduction band offset (ΔE_C) between MgO and ZnO is about 3.55 eV.[25] In this way, the high ΔE_C will generate a barrier that prevents the electrons drifting from ZnO to Pt electrode, thus lead an accumulation of electrons at the interface of MgO/ZnO under a forward bias. In our case, the electric field in the MgO layer is in an order of 10^6 V cm^{-1} at the threshold current due to its excellent dielectric nature. Under such a high electric field, the electrons and holes can be efficiently excited via the impact-ionization mechanism.[25] Therefore, the generated holes in MgO layer can be injected into the ZnO film, thus recombined with the accumulated electrons at the MgO/ZnO interface, which results the observed UV electroluminescence. We have also attempted to interpret the EL based on the tunneling mechanism as reported previously.[29] However, the expression derived from the tunneling process cannot be adequately used to explain our result. Besides, the thickness of the MgO layer of 30 nm is too large for the tunneling action to occur.

Figure 8 shows the EL spectra at different detected angles. The injection current is fixed at a value of 60 mA. Measurement setup is shown by the inset, and θ is defined as the angle between the detector and sample surface. As observed, the lasing spectrum shows a wide angle distribution and reveals one of it display and emitting advantages. The lasing peaks and intensities vary with different angles as shown in Figure 8. The possible origin of the EL intensity variation may be attributed to the randomly distributed cavities inside ZnO nanocrystallite films, thus result different output directions, intensities, and lasing modes observed at various angles. These features are very similar to the optically and electrically pumped random lasers reported in ZnO by Cao et al.[17] and Zhu et al.,[25] which further confirm the existence of random lasers in our RLM device.

Here, we simply propose a facile and practical concept for the elevation of the newly designed RLM device as future outlook. For traditional RRAM device, the data is transmitted by

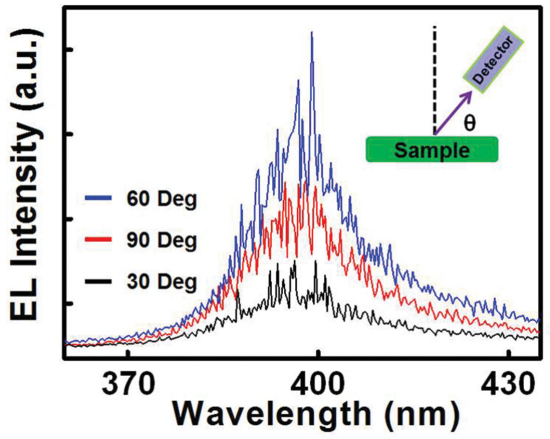

Figure 8. The inset denotes the schematic measurement setup. θ is the angle between sample surface and detector.

scanning one bit after another, thus suffers the drawback of serial sequence of reading process.[29] Therefore, one way to enhance the data transmission is via optical detection, which provides parallel reading process. For instance, when the RLM is turned on, the signal can be collected by an optical sensor, that is, regions without laser are served as logic "0," and regions with laser are served as logic "1." Once when the optical sensor can sense and distinguish each lasing signal derived from RLM at the same time, the maximum data throughput can be greatly enhanced. Besides, the highly coherent lasers exhibit much more advantages than purely spontaneous emission. At the current stage, the RLM device still requires a significant high value of injection current to generate the laser action; it thus suffers a hurdle of time delay to reflect the turn-on phenomenon instantly. Nevertheless, the way of improvement is still undoubtedly modern and fascinating.

3. Conclusions

In summary, we have made the first demonstration of a RLM device. The success of RLM mainly arises from the integration of both functionalities of random lasers and memories. During the characterization, the RLM is found to exhibit a significant high ON/OFF current ratio of $\approx 10^7$, and considerable duration of more than 10^3 s. The random lasing derived from RLM device shows a broad angle distribution with a drive current threshold of about 30 mA. We believe that our approach may promote both laser and RRAM for diversified applications in modern functional electronics and pave a new route to advance the traditional memories using electrical detection by faster parallel optical reading process. In addition, the discovered electrically operated memory device with optical output would open a true application horizon for the realization of all optical memories.

4. Experimental Section

To fabricate the RLM device, the ZnO nano-crystallite films and MgO layer were deposited in sequence onto the ITO glass by using the radio-frequency (RF) magnetron sputtering technique. The ITO glass with the ITO thickness of about 260 nm was previously ultrasonically cleaned for 10 min in acetone, ethanol and deionized (DI) water in sequence to remove any absorbed contaminant. Prior to the MgO sputtering, the ZnO films were post-annealed at 300 °C for 1 h under the air condition in order to reach a better quality. After that, MgO and Pt layer were deposited onto the ZnO films in sequence to form a MIS (Pt/MgO/ZnO) structure. The RF power for sputtering ZnO and MgO films were both 300 W, and the chosen inert gas was Ar. When the sputtering action was started, the pressure inside the cavity was around 4.2×10^{-3} Torr. The Pt layer was deposited by using the direct-current (DC) sputtering system (JFC-1600, JEOL). The thickness of the Pt, MgO, and ZnO layer is 10, 30, and 100 nm, respectively. It is worth noting that the thickness of MgO layer is set at 30 nm, because when the thickness is too large, such as 50 nm, the memory effect will still exist, but the random laser action cannot be obtained duo to the large voltage drop across the MgO layer and less injected charges into ZnO layer. On the contrast, when the thickness of MgO layer is as thin as 10 nm, both memory effect and random laser action disappear. Under this circumstance, the defective MgO layer can easily form a short circuit losing the capability to serve as a blocking layer and the charge carriers cannot be accumulated at the interface and produce radiative recombination.

The morphology of the ZnO films was characterized by scanning electron microscope (JEOL JSM6500). The existence of ZnO was confirmed by the X-ray diffraction with a wavelength of 0.15406 nm (Panalytical X'pert PRO), and photoluminescence (PL) spectra, which were carried out by the excitation of 325 nm He-Cd laser. The current–voltage (*I–V*) and current–time (*I–T*) characteristics of RLM device were measured by using the Keithley 2410 semiconductor parameter analyzer. During the measurement in voltage sweeping mode, the bias was defined as positive when the current flowed from the top to bottom electrode, and defined as negative when the current flowed in opposite direction. EL measurements were carried out in a Jobin Yvon iHR550 imaging spectrometer system with a continuous-current power source. Note that all the measurements were performed at room temperature.

Acknowledgements

This work was supported by the Ministry of Science and Technology and the Ministry of Education of the Republic of China.

Received: February 23, 2015
Revised: April 17, 2015
Published online: May 15, 2015

[1] R. Waser, R. Dittmann, G. Staikov, *Adv. Mater.* **2009**, *21*, 2632.
[2] Y. D. Chiang, W. Y. Chang, C. Y. Ho, C. Y. Chen, C. H. Ho, S. J. Lin, T. B. Wu, J. H. He, *IEEE Trans. Electron. Devices* **2011**, *58*, 1735.
[3] Y. C. Lai, Y. X. Wang, Y. C. Huang, T. Y. Lin, Y. P. Hsieh, Y. J. Yang, Y. F. Chen, *Adv. Funct. Mater.* **2013**, *24*, 1430.
[4] Y. C. Lai, F. C. Hsu, J. Y. Chen, J. H. He, T. C. Chang, Y. P. Hsieh, T. Y. Lin, Y. J. Yang, Y. F. Chen, *Adv. Mater.* **2013**, *25*, 2733.
[5] M. K. Hota, M. K. Bera, B. Kundu, S. C. Kundu, C. K. Maiti, *Adv. Funct. Mater.* **2012**, *22*, 4493.
[6] H. Wang, F. Meng, Y. Cai, L. Zheng, Y. Li, Y. Liu, Y. Jiang, X. Wang, X. Chen, *Adv. Mater.* **2013**, *25*, 5498.
[7] J. H. Yoon, J. H. Han, J. S. Jung, W. Jeon, G. H. Kim, S. J. Song, J. Y. Seok, K. J. Yoon, M. H. Lee, C. S. Hwang, *Adv. Mater.* **2013**, *25*, 1987.
[8] H. H. Huang, W. C. Shih, C. H. Lai, *Appl. Phys. Lett.* **2010**, *96*, 193505.
[9] F. C. Chiu, W. C. Shih, J. J. Feng, *J. Appl. Phys.* **2012**, *111*, 094104.
[10] W. Y. Chang, C. A. Lin, J. H. He, T. B. Wu, *Appl. Phys. Lett.* **2010**, *96*, 242109.
[11] X. Cao, X. M. Li, X. D. Gao, X. J. Liu, C. Yang, R. Yang, P. Jin, *J. Phys. D: Appl. Phys.* **2011**, *44*, 255104.
[12] C. H. Huang, J. S. Huang, S. M. Lin, W. Y. Chang, J. H. He, Y. L. Chueh, *ACS. Nano* **2012**, *6*, 8407.
[13] J. Qi, M. Olmedo, J. G , Zheng, J. Liu, *Sci. Rep.* **2013**, *3*, 2405.
[14] A. Manekkathodi, M. Y. Lu, C. W. Wang, L. J. Chen, *Adv. Mater.* **2010**, *22*, 4059.
[15] H. Noh, J. K. Yang, S. F. Liew, M. J. Rooks, G. S. Solomon, H. Cao. *Phys. Rev. Lett.* **2011**, *106*, 183901.
[16] M. Leonetti, C. Conti, C. Lopez, *Nat. Photonics* **2011**, *5*, 615.
[17] H. Cao, Y. G. Zhao, S. T. Ho, E. W. Seelig, Q. H. Wang, R. P. H. Chang, *Phys. Rev. Lett.* **1999**, *82*, 2278.
[18] J. Huang, S. Chu, J. Y. Kong, L. Zhang, C. M. Schwarz, G. P. Wang, L. Chernyak, Z. H. Chen, J. L. Liu, *Adv. Opt. Mater.* **2013**, *1*, 179.
[19] D. S. Wiersma, S. Cavalieri, *Nature* **2001**, *414*, 708.
[20] R. M. Balachandran, D. P. Pacheco, N. M. Lawandy, *Appl. Opt.* **1996**, *35*, 640.
[21] R. C. Polson, Z. V. Vardney, *Appl. Phys. Lett.* **2004**, *85*, 1289.
[22] M. Sakai, Y. Inose, K. Ema, T. Ohtsuki, H. Sekiguchi, A. Kikuchi, K. Kishino, *Appl. Phys. Lett.* **2010**, *97*, 151109.

[23] B. L. Cao, Y. Jiang, C. Wang, W. H. Wang, L. Z. Wang, M. Niu, W. J. Zhang, Y. Q. Li, S. T. Lee, *Adv. Funct. Mater.* **2007**, *17*, 1501.
[24] H. Zhu, C. X. Shan, B. Yao, B. H. Li, J. Y. Zhang, Z. Z. Zhang, D. X. Zhao, D. Z. Shen, X. W. Fan, Y. M. Lu, Z. K. Tang, *Adv. Mater.* **2009**, *21*, 1613.
[25] H. Zhu, C. X. Shan, J. Y. Zhang, Z. Z. Zhang, B. H. Li, D. X. Zhao, B. Yao, D. Z. Shen, X. W. Fan, Z. K. Tang, X. H. Hou, K. L. Choy, *Adv. Mater.* **2010**, *22*, 1877.
[26] S. Chu, G. P. Wang, W. H. Zhou, Y. Q. Lin, L. N. Chernyak, J. Z. Zhao, J. Y. Kong, L. Li, J. J. Ren, J. L. Liu, *Nat. Nanotechnol.* **2011**, *6*, 506.
[27] Q. Qiao, C. X. Shan, J. Zheng, H. Zhu, S. F. Yu, B. H. Li, Y. Jiae, D. Z. Shen, *Nanoscale* **2013**, *5*, 513.
[28] C. S. Wang, T. Y. Chang, T. Y. Lin, Y. F. Chen, *Sci. Rep.* **2014**, *4*, 6736.
[29] C. W. Chang, W. C. Tan, M. L. Lu, T. C. Pan, Y. J. Yang, Y. F. Chen, *Sci. Rep.* **2014**, *4*, 5121.